UNIVERSITY OF CALIFORNIA, SAN DIEGO

Morphology of CDKL5 iPSC-derived neurons and rescue of synaptic and functional defects

A Thesis submitted in partial satisfaction of the requirements for the degree
Master of Science

in

Biology

by

Nicholas Liang

Committee in charge:

Alysson R. Muotri, Chair
Brenda Bloodgood, Co-Chair
Lisa McDonnell

2017

The Thesis of Nicholas Liang is approved, and it is acceptable in quality and form for publication on microfilm and electronically:

_____

_____

Co-Chair

_____

Chair

University of California, San Diego

2017

DEDICATION

I dedicate this thesis to my loving family - from my parents, who have sacrificed so much to give me a better life, to my Aunt Jessica and Stephanie and Uncle Richard, who have always been like second parents to me. Thank you for your constant and unwavering support and your unconditional love. I love you all and hope to make you proud.

TABLE OF CONTENTS

LIST OF ABBREVIATIONS

CDKL5 - cyclin-dependent kinase-like 5

iPSCs - induced pluripotent stem cells

NPCs - neural progenitor cells

HDAC4 - histone deacetylase 4

hESCs - human embryonic stem cells

SCNT - somatic cell nuclear transfer

RTT - Rett syndrome

MeCP2 - methyl-CpG-binding protein 2

IGF1 - insulin-growth factor 1

DNMT1 - DNA methyltransferase 1

BDNF - brain-derived neurotrophic factor

NGL-1 - netrin-G1 ligand

PSD95 - postsynaptic density protein 95

CTL - control

EBs - embryoid bodies

Syn - Synapsin 1

MEA - multi-electrode array

H&E - haemotoxylin & eosin

Map2 - microtubule-associated protein 2

HuNu - human nuclear antigen

CF - cystic fibrosis

CFTR - CF transmembrane conductance regulator

LIST OF FIGURES

LIST OF TABLES

ACKNOWLEDGEMENTS

I would like to acknowledge Alysson R. Muotri for the privilege and opportunity to take part in the research we do in the lab. The Muotri Lab has been an integral part of my amazing experience here at UCSD and it would not have been possible without Alysson, the post-docs, grad students and other lab members.

Next, I would like to thank Brenda Bloodgood and Lisa McDonnell for not just their time and effort to be on my committee, but also for being educators truly invested in the learning experience of undergraduates at UCSD. My opportunities to learn and interact with students under their instruction has imparted upon me the importance of undergraduate education, which has been crucial in my work as a graduate student.

Lastly, I would like to thank Cleber Trujillo and Pri Negraes for everything they have taught me about research and beyond. Prior to working with them, I was unsure about my career goals nor did I have any clue the rigors and commitment of scientific research. These last couple years, with their guidance and mentorship, I have learned so much and matured greatly. As I prepare for my defense, I look back at the long way I have come and can only imagine the patience and effort they have invested in me, which I am forever grateful.

ABSTRACT OF THE THESIS

Morphology of CDKL5 iPSC-derived neurons and
rescue of synaptic and functional defects

by

Nicholas Liang

Master of Science in Biology

University of California, San Diego, 2017

Professor Alysson R. Muotri, Chair

Professor Brenda Bloodgood, Co-Chair

Cyclin-dependent kinase-like 5 (CDKL5) syndrome is a neurodevelopmental disorder characterized by early-onset intractable seizures, mental retardation, and hand stereotypies. Studies have shown that loss of CDKL5 protein function is responsible for aberrations in neuronal morphogenesis, and decreased synaptogenesis. In order to understand the effects of *CDKL5* mutations on human neural disease pathology, we utilized induced pluripotent stem cell (iPSC) technology to generate human iPSC-derived neurons from CDKL5 patients. Furthermore, to circumvent *in vitro* iPSC disease modeling limitations and to take advantage of an *in vivo* brain environment, we integrated

these two systems by engrafting human iPSC-derived neural progenitor cells (NPCs) into immunodeficient mice. Here, we report defects in neuronal morphology in CDKL5-mutant neurons differentiated *in vitro* that are retained in human neurons differentiated in a mouse brain. Furthermore, we found that using a histone deacetylase inhibitor LMK235, specific to histone deacetylase 4 (HDAC4), was able to rescue defects in synaptogenesis and neural electrical activity in CDKL5 iPSC-derived neurons *in vitro*. Ultimately, we hope our work will provide further insights into CDKL5 disease pathology and accelerate the development of treatments for this complex neurodevelopmental disorder.

INTRODUCTION

Disease modeling

A disease model requires an organism that is able to recapitulate some of the pathological processes observed in human disease. From flies to higher order organisms, such as mice or chimps, there are a variety of animals used to aid in the understanding of disease pathogenesis and its physical manifestation. Animal models have provided significant insight into the roles of specific genes, and molecular and cellular signaling pathways (Johnston, 2005). The use of non-human models enables advances in understanding disease etiology without compromising the life of an actual human being. Mice, for example, are one of the most commonly used model organisms that serve a range of applications. However, there are major differences in development and structure between humans and mice (Watase and Zoghbi, 2003). Mice cortices are unfolded and lissencephalic while human cortices have grooves giving rise to sulci and gyri. Therefore, care must be taken when extrapolating information between organisms due to inherent limitations imposed by interspecies differences.

Animal models are valuable for studying monogenic disorders provided that the afflicted gene will accurately mimic the dysregulated cellular interactions of the human disease; however, genes may display differential functions across species, limiting the use of genome-edited animal models to accurately recapitulate human diseases (Liang et al., 2017). Notable investments have been made to clarify disease mechanisms and unveil prospective therapies, but the outcomes have been modest (Dragunow, 2008).This is apparent in the low percentage of drugs that have shown improvement in pre-clinical animal models, but rarely pass human clinical trials (<10%). An alternative to investigating neurological illnesses is post-mortem brain tissue, but it only provides an

end-stage snapshot of alterations in brain structure at both cellular and molecular levels. Furthermore, post-mortem brain tissue does not provide any temporal or mechanistic insights into disease pathogenesis, are scarce and the tissue integrity may be compromised from the storage and handling. Therefore, it is important to use a more suitable preclinical model able to faithfully mimic the pathophysiology of human disease processes and to serve as a platform for target identification and therapeutic approaches.

Induced pluripotent stem cell (iPSC) derived neurons and their application

Pluripotent human embryonic stem cells (hESCs) have been successfully generated from early stage human embryos and can differentiate *in vitro* and *in vivo* into various cell types (Thomson et al., 1998). However, to develop cellular models of human disease, it is necessary to generate new cell lines with genomes pre-disposed to disease. Although somatic cell nuclear transfer (SCNT) is a rapid process that yields ESCs, the ethical complications and unknown mechanism of reprogramming diminish its utility. In 2007, through overexpression of four transcription factors, Takashi and coworkers were able to generate ESC-like cells, known as iPSCs (Takahashi et al., 2007). Due to their potential to terminally differentiate into cell types from the three germ layers after exposure to a specific cocktail of growth factors and culture conditions, iPSCs presented a more viable option for many applications such as cellular transplantation and disease modeling (Takahashi et al., 2007; Thomson et al., 1998). The development of iPSCs and neural differentiation protocols have allowed, for the first time, the ability to generate live human neurons, allowing for the study of neural networks from patients with genomes predisposed to disease.

The similarity between *in vitro* pluripotent stem cell-derived neural cultures and the human brain remains a fundamental concern to model neurological disorders. To better understand how closely *in vitro* neural cultures mimic the human brain, Stein and coworkers employed an array of unbiased, comprehensive and quantitative methods to identify the regional identity and developmental maturity of hiPSC-derived neurons (Stein et al., 2014). Gene expression analysis revealed an enrichment in cortical regional markers while expression of markers from other brain regions was much lower, illuminating the cortical identity of *in vitro* cultures (Stein et al., 2014). Furthermore, it was revealed that hiPSC-derived neurons never matured beyond mid-fetal stages in a dish. Despite these limitations, multiple analytical approaches and independent data sets still revealed that *in vitro* differentiation strongly matched *in vivo* development with most neurodevelopmental processes of corticogenesis being preserved (Stein et al., 2014). This study revealed that cells generated from *in vitro* differentiation of NPCs are enriched for cortical neurons, which may limit studies where there are non-cortical neuronal subtypes afflicted. The developmental maturity that *in vitro* cultures attain may also limit the use of iPSC-derived neurons for late-onset diseases. Nonetheless, the high preservation of neurodevelopmental processes will be useful in modeling neurodevelopmental disorders.

Studying human neurodevelopment *in vivo* remains largely unexplored due to the paucity of experimental models, but has major implications for understanding brain development and neurological diseases. To circumvent limitations of *in vitro* experimental models and to take advantage of human iPSCs and ESCs, Muotri and coworkers engrafted human ESCs into neonatal mouse brains; these cells successfully differentiated into neurons and integrated robustly into the mouse neural circuitry (Muotri

et al., 2005). Moreover, the engrafted cells displayed progressive complexity, ultimately yielding functional synapses within the mouse neural circuitry. The robust integration and progressive development of these human cells over time show that engrafted human neurons are able to follow intrinsic molecular signaling cues in the context of a mouse brain environment. The preservation of mouse intrinsic pathways in human cells offers an unprecedented opportunity for modeling human neurodevelopment and disease in the context of an *in vivo* brain environment.

Using iPSCs to model a neurodevelopmental disorder

The advent of iPSCs has already provided novel information in the study of disease phenotypes, neurodevelopment, and therapy discovery. In 2010, Marchetto and coworkers developed one of the first human iPSC disease models for the neurodevelopmental disorder, Rett syndrome (RTT) (Marchetto et al., 2010). RTT is a neurodevelopmental disorder due to mutations in the *MECP2* gene, encoding the transcriptional regulator protein, methyl-CpG-binding protein 2 (MeCP2). The authors reprogrammed and differentiated fibroblasts derived from RTT patients to generate iPSC-derived neurons. Their work confirmed prior mouse and patient post-mortem brain results, as human RTT neurons displayed a reduced number of excitatory synapses and smaller soma sizes. Taking advantage of this human model to screen potential compounds, insulin-growth factor 1 (IGF1) was administered to iPSC-derived RTT neurons. IGF1 had previously been reported to promote a partial reversal of RTT-like symptoms in a mouse model (Tropea et al., 2009). IGF1-treated RTT neurons exhibited an increase in glutamatergic synapse number, displaying a developmental window of rescue where RTT neurons are amenable to pharmacological intervention. Altogether,

these findings serve as a proof-of-principle that iPSC-derived neurons are capable of maintaining neurological deficits displayed in *in vivo* animal models and post-mortem brain tissue, validating iPSC-derived neural cells as a suitable model to recapitulate neurodevelopmental disorders. Furthermore, these results show that iPSC-derived neurons can be used as an alternative preclinical platform for drug screening.

CDKL5 disorder

In humans, mutations in the *CDKL5* gene lead to symptoms such as early-onset intractable seizures as well as RTT-like features such as mental retardation, deceleration of head growth and hand stereotypies. Due to overlapping symptoms with RTT, CDKL5 disorder was initially misdiagnosed as an early-onset seizure variant of RTT (Hanefield variant), which may be attributed to CDKL5 and MeCP2 acting on a common molecular pathway. Recent advances in DNA sequencing technology and further knowledge of the gene and its function have revealed CDKL5 disorder to be independent of RTT (Fehr et al., 2012). Due to its location on the X-chromosome, the disorder predominantly affects females, while ~10% of cases affect males; there have been ~600 cases reported worldwide. Hemizygous males potentially will display a more severe phenotype, due to the absence of a functional copy of CDKL5, whereas, females present with a spectrum of clinically heterogeneous phenotypes due to either a mosaicism of mutant CDKL5 X-inactivation, or the severity of the CDKL5 mutation.

Cyclin-dependent kinase-like 5 (CDKL5) gene, function and models

CDKL5 is a kinase that is essential for brain maturation and synaptogenesis and is located at the Xp22.13 locus. Currently, the known downstream phosphorylation targets of CDKL5 are MeCP2, DNA methyltransferase 1 (DNMT1), and HDAC4 (Kameshita et

al., 2008; Mari et al., 2005; Trazzi et al., 2016). Consisting of 24 exons, it is a fairly large gene and multiple isoforms have been described to exist in various tissues (Fichou et al., 2011; Hector et al., 2016; Kalscheuer et al., 2003; Williamson et al., 2012). In the brain, CDKL5 is primarily found in neurons, but it has been detected in glial cells at significantly lower levels (Chen et al., 2010; Rusconi et al., 2008). It appears to be highly modulated at the regional level in the brain, showing enrichment in forebrain regions such as the striatum, cortex, and hippocampus (Chen et al., 2010; Rusconi et al., 2008; Wang et al., 2012). The protein is present in various other tissues such as liver, lung, thymus, spleen, and testis (Chen et al., 2010; Lin et al., 2005). Temporally, CDKL5 protein expression is initially low in the embryonic rodent brain and primarily localized in the cytoplasm and becomes strongly induced in late prenatal to early postnatal stages, plateauing around postnatal day 14 (P14), suggesting the importance of CDKL5 during early brain development (Chen et al., 2010; Rusconi et al., 2008). Following P14 to adult stages, a slow decline of CDKL5 expression is observed and the distribution becomes almost even between the nucleus and cytoplasm (Chen et al., 2010; Rusconi et al., 2008).

In the cytoplasm, CDKL5 has been shown to be an important regulator of neurite outgrowth and synapse formation. In the absence of CDKL5, rat cortical neurons displayed a decrease in total dendrite length and arborization *in vitro* (Chen et al., 2010). Furthermore, knock-down of CDKL5 in rat brains *in vivo* resulted in a decrease in total neurite length in layer II/III pyramidal neurons. The mechanism that CDKL5 is able to influence neuronal morphogenesis is by inducing Rac-1, a critical regulator of actin remodeling and neuronal morphogenesis, signaling through activation by brain-derived

neurotrophic factor (BDNF), a critical regulator of neuronal development and function (Chen et al., 2010; McAllister et al., 1995).

The precise role that CDKL5 plays in synapse formation remains to be elucidated, but it has been shown to be critical for the maintenance of synaptic contacts, as demonstrated *in vitro* and *in vivo* in mouse primary neurons and human iPSC-derived neurons *in vitro* (Ricciardi et al., 2012). CDKL5 was shown to localize in dendrites, almost exclusively at excitatory spines and knocking down CDKL5 resulted in less excitatory synapses in mouse models. Furthermore, CDKL5 patient iPSC-derived neurons also displayed less excitatory synapses *in vitro*. The mechanism of CDKL5 is regulated by the phosphorylated state of netrin-G1 ligand (NGL-1), a synaptic cell adhesion molecule, and thereby, its ability to bind postsynaptic density protein 95 (PSD95), a synaptic protein localized at the post-synaptic density, and stabilize their association (Ricciardi et al., 2012). CDKL5 has also been shown to directly bind palmitoylated PSD95, which promotes targeting of CDKL5 to excitatory synapses (Zhu et al., 2013).

Although the precise biological function of CDKL5 remains to be elucidated, it is known to be crucial for neuronal morphogenesis and formation of excitatory synapses. Unique knock-out mouse models of CDKL5 have been generated and display the majority of symptoms in human patients such as hyperactivity, motor defects, reduced anxiety, decreased sociability and impaired learning and memory, which may mimic the hand stereotypies, intellectual disability, hyperactivity, and the poor response to social interactions (Amendola et al., 2014; Wang et al., 2012). However, one major exception is that these mice are unable to recapitulate the spontaneous seizures.

MATERIALS AND METHODS

Patient consent

Control (CTL) and CDKL5 fibroblasts were obtained from explants of dermal biopsies following informed consent under protocols approved by the University of California San Diego Institutional Review Board (#141223ZF). For more patient information, please refer to **Table 1**.

Animal protocol and consent

NOD.CB17-*Prkdc*^{scid}/NcrCrl mice were purchased from Charles River Laboratories and bred in the vivarium of Sanford Consortium for Regenerative Medicine. Mice were provided enrichment, kept in standard dark/light cycle conditions and housed under standard requirements of rodent IACUC guidelines (one to five individuals per cage). All animal experiments were performed in accordance with relevant guidelines and regulations, and approved by the Institutional Animal Care and Use Committee (IACUC) at the University of California San Diego (protocol S09005).

Neural induction and neuronal differentiation

iPSCs were cultured on matrigel-coated dishes (BD Bioscience, San Jose, California) and fed daily with mTeSR1 (StemCell Technologies). To begin neural induction, mTeSR media was switched to N2 medium (DMEM/F12 50/50 (Corning Cellgro) with HEPES, Pen Strep (Life Technologies), GlutaMAX (Life Technologies), and N2 NeuroPlex (Gemini Bio-Products)), supplemented with 1 μM dorsomorphin (Tocris) and 10 μM SB431542 (Stemgent)), for 1-2 days. iPSC colonies were then lifted off, cultured in suspension on the shaker (95 r.p.m. at 37°C) for eight days to form embryoid bodies (EBs) and fed with N2 media. EBs were then mechanically dissociated, plated on a matrigel-coated dish and fed with N2Gem21 medium (DMEM/F12 50/50

(Corning Cellgro) with HEPES, Pen Strep (Life Technologies), GlutaMAX (Life Technologies), N2 NeuroPlex (Gemini Bio-Products) and Gem21 NeuroPlex (Gemini Bio-Products)) and 20 ng/mL FGF-2. The emerging rosettes were picked manually, dissociated completely using StemPro Accutase (Life Technologies) and plated on a poly-ornithine/laminin-coated plate. NPCs were expanded in N2Gem21 medium, supplemented with 20 ng/mL FGF-2, and fed every other day. To differentiate NPCs into neurons, FGF-2 was withdrawn from the N2Gem21 medium. To differentiate NPCs into neurospheres, NPCs were lifted off and dissociated using StemPro Accutase (Life Technologies). Then, NPCs were cultured in suspension while shaking for 4 weeks in N2Gem21 medium.

Immunocytochemistry

Cells were washed with Dulbecco's Phosphate-Buffered Saline (DPBS, Corning Cellgro) three times (5 min each), fixed in 4% paraformaldehyde (PFA, Electron Microscopy Sciences) for 20 min, washed with DPBS three times (5 min each), and incubated in blocking/permeabilizing solution (0.1% Triton X-100, 3% BSA (Gemini Bio-Products, 700-110)) for 30 min at room temperature. Primary and secondary antibodies were diluted in blocking/permeabilizing solution. Cells were incubated in the primary antibody overnight at 4°C. The next day, cells were washed with DPBS three times (5 min each), incubated with secondary antibodies for 1 hour at room temperature and washed with DPBS three times (5 min each). Nuclei were stained using DAPI (1:10,000). Slides or coverslips were mounted using Prolong Gold antifade mountant (Life Technologies).

Primary antibody for immunocytochemistry dilutions were used as follows: anti-Tra1-60 (Company, catalogue number, 1:250), anti-Oct4 (,1:500), anti-Nestin (Millipore, ABD69, 1:250), anti-Sox2 (Abcam, ab75485, 1:250), anti-GFAP (Abcam, ab4674, 1:2000), anti-Map2 (Abcam, ab3392, 1:2000), anti-Vglut1 (1:500), anti-Homer1 (1:500). Secondary antibodies conjugated to Alexa Fluors 488, 555, 647 were used with a dilution of 1:1000 (Life Technologies).

Teratoma assay

Dissociated iPSC colonies were pelleted and resuspended in 1:1 matrigel and DPBS. Around 1-3 x 10^6 cells were injected subcutaneously in in the lower hind leg of nude mice. After 1-2 months, teratomas were dissected, fixed and sliced. Sections were stained with haematoxylin and eosin (H&E) for further analysis.

Quantification of Map2-positive cells

Neurons were differentiated for 8 weeks and immunostained for microtubule-associated protein 2 (Map2) and DAPI (refer to Immunocytochemistry of MATERIALS AND METHODS for details of immunostaining). Percentage of Map2-positive cells were determined by number of cells co-expressing Map2 and DAPI divided by total number of DAPI nuclei.

Lentivirus transduction

hiPSC-derived NPCs were transduced with Synapsin-1 (Syn) promoter upstream of a EGFP reporter in a lentivirus backbone (Nageshappa et al., 2015). Transduction M.O.I. was approximately 2.

Morphometric analysis of iPSC-derived neurons

Neurons transduced with Syn::GFP lentivirus were differentiated for 8 weeks, stained with GFP and traced using Neurolucida version 9 (MBF Bioscience, Williston, VT) connected to a Zeiss Axio Imager 2 microscope with a 40 x oil objective. Neurons were traced provided that they had an ovoid-shaped soma and at least two neurites (dendrites) that were each at least double the length of the soma. The neurites were considered dendrites based on the following criteria: (1) thickness that decreased with the distance from the cell body; and (2) branches emerging under acute angle. In addition, only enhanced-GFP-positive neurons with dendrites displaying evenly distributed fluorescent stain along their entire length, were included in the analysis. The morphology of the neurons was quantified along *x*-, *y*-, and *z*- coordinates using Neurolucida Explorer version (MBF Bioscience, Williston, VT). No distinction was made between apical and basal dendrites, and the results reflect summed length of all neurites/dendrites per neuron To minimize the effects of cutting on dendritic measurements, we included neurons with cell bodies located near the center of an 80-μm-thick histological sections, with natural terminations of higher-order dendritic branches present where possible. Inclusion of the neurons completely contained within 80-μm section biases the sample towards smaller neurons, leading to the underestimation of dendritic length; therefore, we applied the same criteria blinded across all CTL and CDKL5 specimens.

Sholl analysis

Analysis was done by using Neurolucida Explorer's Sholl Analysis option, which specified a center point in the middle of the soma, surrounded by a grid of concentric rings of radii increasing in increments of 10 μm. The number of intersections at each ring is recorded to indicate neuronal complexity.

***In vivo* grafting, perfusion and brain collection**

Neonatal mice were anesthetized by hypothermia prior to grafting. Approximately 2×10^4 EGFP-positive NPCs in 1 μl of PBS were stereotaxically injected 2 mm from the midline between the Bregma and Lambda and 1-2 mm deep into the lateral ventricles of each mouse with the help of a microglass capillary connected to a Hamilton syringe. Six months after grafting, the host animals were anesthetized via i.p. injection of ketamine then transcardially perfused with ice cold PBS, followed by 4% PFA. After extraction, brains were fixed in 4% PFA for 48 h, then 30% sucrose for an additional 48 h. Brains were sectioned at a thickness of 80-μm coronally on a freezing microtome and immediately stained immunohistochemically afterwards.

Mouse brain sections immunohistochemistry

Free-floating brain sections were washed twice with DPBS (5 min each). After washing, brain sections were incubated in blocking/permeabilizing solution (0.1% Triton X-100, 3% FBS (Gibco, 12676011) for 2 h at room temperature. Primary and secondary antibodies were diluted in blocking/permeabilizing solution. Brain slices were incubated in primary antibodies while shaking for 48 h at 4°C. Two days later, slices were washed with DPBS three times (5 min each), incubated with secondary antibodies for 2 h at room temperature and washed with DPBS three times (5 min each). Nuclei were stained using DAPI (1:10,000) for 10 min and mounted onto glass slides. DPX mountant (Sigma-Aldrich, 06522) was added to slides then coverslipped. Primary antibodies for immunohistochemistry dilutions were used as follows:

anti-HuNu (Millipore, mab1281, 1:1500), anti-GFP (Abcam, ab13970, 1:2000). Secondary antibodies conjugated to Alexa Fluors 488, 555, 647 were used with a dilution of 1:1000 (Life Technologies).

Drug Treatment Conditions

For cells screened with read-through compounds (PTCA's, RTC13, Gentamicin), NPCs were differentiated for 4 weeks in N2Gem21 media, the drugs were added and cells were snap-frozen 48 h later. For drug concentrations, please refer to **Table 2**.

For cells treated with synaptogenesis and neural activity rescue drugs (Tideglusib, Nefiracetam, IGF-1, LiCl, LMK235), NPCs were differentiated for 4 weeks in N2Gem21 media. Following this, cells were chronically treated for 4 weeks in N2Gem21 media. Media was changed twice a week. Please refer to **Table 2** for drug concentrations.

Synaptic puncta quantification

NPCs were differentiated for 8 weeks in N2Gem21 media in the absence of FGF-2 then stained for the following markers: Vglut1, Homer1, and Map2 (refer to Immunocytochemistry for protocol). Co-localized Vglut1 (presynaptic) and Homer1 (postsynaptic) puncta were quantified after three-dimensional reconstruction of z-stack random images for CTL and CDKL5 conditions. Slides were analyzed under a fluorescence microscope (Z1 Axio Observer Apotome Zeiss). Only puncta in proximity of Map2-positive processes were scored.

Western blotting

Neurons were lysed in RIPA buffer with protease inhibitor, incubated at 4°C for 15 min, and centrifuged for 15 min at 14,000g at 4°C. Protein concentration of the supernatant was determined using bovine serum albumin (BSA) as a standard (Pierce

BCA Protein Assay Kit (Thermo Scientific, 23225). Protein supernatant was boiled at 95°C for 10 min, separated by SDS-PAGE (Bolt 4-12% Bis-Tris Plus) and blotted to nitrocellulose membrane (iBlot 2 Transfer Stacks, IB23001). Membranes were blocked in blocking solution (Rockland, MB070) for 4 h at room temperature. Primary and secondary antibodies were diluted in blocking solution. Membranes were incubated in primary antibody for 16 h at 4°C while shaking, washed with PBS + 0.1% Tween five times (5 min each), then incubated in the secondary antibody for 1 h. Finally, samples were washed with PBS + 0.1% Tween five times (5 min each). The Odyssey system was used for signal detection. Signal intensities were measured using the Image Studio software for semi-quantitative analysis, normalized to β-actin. Primary antibody for Western blotting dilutions were used as follows:
anti-CDKL5 (Santa Cruz Biotechnology, sc-376314, 1:500), anti-β-actin (Abcam, ab8227, 1:10,000), anti-Synapsin1 (Millipore Sigma, ab1543p, 1:1500), anti-PSD95 (Antibodies Inc., 75-028, 1:1500), anti-Tubulinβ3 (Biolegend, MMS435P, 1:10,000), anti-GFP (ThermoFisher Scientific, A11122, 1:2000) . IRDye800CW and IRDye680RD were used as secondary antibodies (Li-Cor, 926-32211, 1:5000).

Multi-electrode array (MEA)

Using 12-well MEA plates from Axion Biosystems, approximately 10,000 NPCs were seeded into each well that was pre-coated with poly-L-ornithine and laminin, then induced into neuronal differentiation for 4 weeks and treated with various compounds for 4 weeks. Cells were fed twice a week and measurements were taken one day after the media was changed. Recordings were performed using a Maestro MEA system and AxIS software (Axion Biosystems), using a band-pass filter with 10 Hz and 5 kHz cutoff

frequencies. Spike detection was performed using an adaptive threshold to set 5.5 times the standard deviation of the estimated noise on each electrode. Each plate first rested for 3 min in the Maestro, and then 3 min of data were recorded to calculate the spike rate per well. MEA analysis was performed using the Axion Biosystems Neural Metrics Tool, wherein electrodes that detected at least five spikes per min were classified as active electrodes. Bursts were identified in the data recorded from each individual electrode using an adaptive Poisson surprise algorithm. Network bursts were identified for each well, using a non-adaptive algorithm requiring a minimum of five spikes with a maximum inter-spike interval of 100 ms.

Statistical analysis

No statistical methods were used to determine sample sizes. For iPSC experiments, 10 cell lines were used for CTL and CDKL5 groups. Data distribution was assumed to be normal. All data were prepared for analysis with standard spreadsheet software (Microsoft Excel). All errors bars shown in the figures are s.e.m. Statistical analysis was done using GraphPad Prism v6 (GraphPad Software Inc., La Jolla, CA). For ANOVA analysis involving multiple sample comparisons, we performed Bonferroni *post hoc* testing to discriminate significance relationships. For *t*-test analysis, we applied two-tailed unpaired tests with alpha-value of 0.05. To determine outliers, a Grabbs' test (Extreme Studentized Deviate) was performed (α=0.05) and significant values were excluded from the analysis.

RESULTS

Characterization of differentiation potential of CDKL5 disorder patient-derived iPSCs

For this study, ten cell lines were used comprising of CDKL5 disorder patients and either their isogenic controls (some female patients) or their family-related controls (**Table 1**). Isogenic cell line pairs were genetically identical with the exception of the *CDKL5* locus to ensure confidence in linking genotype to phenotype. Patient mutations comprised of premature nonsense mutations leading to no expression of the CDKL5 protein or one patient with a splicing mutation, leading to the skipping of exon 7 (**Fig. 1a, Table 1**). To induce neurogenesis, the media was changed to N2 supplemented with dorsomorphin and small molecule SB431542, to inhibit mesodermal and endodermal fates (**Fig. 1b**) (Chambers et al., 2009). iPSC colonies were lifted off the plates and transferred to a 6-well plate on a shaker in non-adherent conditions for embryoid body (EB) formation (**Fig. 1b**). After eight days, EBs were plated and the media was changed to N2Gem21 supplemented with FGF-2 for neuroectodermal rosette formation (**Fig. 1b**). Seven days later, neuroectodermal rosettes were formed, mechanically picked and dissociated to allow separation of single NPCs. NPCs were expanded and to promote neuronal differentiation, FGF-2 was removed from the N2Gem21 medium for varying periods of time (**Fig. 1b**).

To characterize the generation of relevant cell types from somatic CDKL5 disorder patient cells, iPSCs and subsequent cell types (NPCs, glutamatergic neurons) were stained and visualized. The presence and localization of stage-specific cell-type markers confirmed the successful generation of iPSCs and derived cell types (**Fig. 1c, e, f**). To assess the pluripotent potential of the iPSCs, immunodeficient mice were

subcutaneously injected with iPSCs in their hind limbs. After 2 months of maturation, iPSC-derived teratomas were extracted for H&E staining. Histological analysis of teratoma tissue-morphology confirmed the presence of tissues representative of all three germ layers, demonstrating the *in vivo* pluripotency of the iPSCs (**Fig. 1d**). Lastly, to determine the consistency and percentage of neurons present in cultures between CTL and CDKL5 disorder iPSC-derived neural cultures, the percentage of Map2-positive cells was quantified. We detected no difference in the percentage of Map2-positive cells between the two conditions, indicating both CTL and CDKL5 lines have similar capabilities to generate neurons. (**Fig. 1g**).

Altered morphology of CDKL5 disorder iPSC-derived neurons *in vitro*

It has been shown that CDKL5 is highly expressed during perinatal development and enriched in forebrain regions such as the cortex (Chen et al., 2010; Rusconi et al., 2008; Wang et al., 2012). With this knowledge and the high expression of CDKL5 during perinatal development and the developmental maturity and regional identity of *in vitro* iPSC-derived neurons (Stein et al., 2014), we decided to differentiate iPSC-derived NPCs. Prior to differentiation, NPCs were transduced with a Syn::EGFP lentivirus in order to track and visualize the complete neuronal morphology. Then, taking advantage of the Muotri lab *in-vitro* differentiation protocol, which predominantly gives rise to cortical neurons of mid-fetal maturity, NPCs were differentiated in order to investigate neuronal morphology in iPSC-derived cortical neurons (Chailangkarn et al., 2016; Marchetto et al., 2010; Stein et al., 2014). NPCs were differentiated for 8 weeks, fixed and immunocytochemistry was performed for GFP to visualize neuronal morphology

(**Fig. 2a**). After morphometric analysis, it was found that human CDKL5 neurons have larger cell body areas and total dendrite lengths compared to CTL (**Fig. 2b, 2c, 2e**). However, no differences were observed in other morphometric parameters (**Fig. 2d, 2f-j**). To investigate dendritic complexity in CDKL5 disorder iPSC-derived neurons, we used Sholl analysis (**Fig. 2k, 2l**). Our data indicates that CDKL5 neurons are significantly more complex compared with CTL (**Fig 2k, 2l**).

Altered morphology of CDKL5 disorder iPSC-derived neurons *in vivo*

Engraftment and differentiation of human cells into a mouse brain has been previously reported and implicated as an unprecedented opportunity for the study of human neurological disorders in the context of an *in vivo* brain environment (Espuny-Camacho et al., 2013; Muotri et al., 2005). Due to limitations in developmental maturity and to take advantage of an *in vivo* brain environment, we decided to integrate these two systems by engrafting human iPSC-derived NPCs into immunodeficient mouse brains. Prior to engraftment, NPCs were transduced with a Syn::EGFP lentivirus in order to track and visualize the complete neuronal morphology of transplanted neurons (**Fig. 3a**). Mouse brains were sectioned coronally and subject to immunohistochemical analysis for markers Human Nuclear Antigen (HuNu) and GFP. Human cells were successfully detected in various regions of the brain and able to differentiate into neurons (**Fig. 3b, c**). After morphometric analysis, human CDKL5 neurons displayed significantly higher total dendritic lengths (**Fig. 3f**) but no differences in other morphometric parameters (**Fig. 3e, g-k**). In order to investigate differences in dendritic complexity, we used Sholl analysis.

Our human-mouse chimera data indicates that CDKL5 neurons are more arborized compared to CTL neurons, which validates our *in vitro* results.

In vitro drug treatment of hiPSC-derived neurons

In addition to using patient-specific neurons for disease modeling, iPSC technology represents a unique platform for drug screening relevant human cell types while overcoming interspecies limitations. hiPSC-derived neurons were screened for various compounds with the goal of recovering the CDKL5 protein, rescuing synaptogenesis and neural activity (**Fig. 4a**). First, a variety of compounds that promote ribosomal read-through of nonsense codons was screened on CDKL5 neurons with the goal of recovering the CDKL5 protein; these read-through drugs are only applicable for genes with nonsense mutations and have been shown to partially recover the absent protein as well as partial functional recovery (Henderson et al., 2012; Tan et al., 2011). An array of compounds was screened in our neural cultures that were differentiated for 4 weeks, exposed to the drugs and collected 48 hours later (acute treatment) (**Table 2**). All patient cell lines used in this study contained nonsense mutations at the *CDKL5* locus, leading to no expression of the protein (**Fig. 4b, 4c, Table 1**). Qualitatively, CDKL5 neurons did not display any discrete band representing the CDKL5 protein (**Fig. 4b**). Upon semi-quantification of the Western Blot, almost no CDKL5 protein was detected, therefore, we did not proceed further with this experiment (**Fig. 4c**).

Loss of CDKL5 has been shown to decrease synaptogenesis in both hiPSC-derived neurons and rodent models (Ricciardi et al., 2012; Trazzi et al., 2016). Various compounds were screened on neural cultures that were differentiated *in vitro* for 4 weeks,

then chronically treated for 4 weeks, followed by immunofluorescent staining of neuron specific-marker Map2, pre-synaptic marker (Vglut1) and post-synaptic markers (Homer1), with the goal of rescuing synapse formation (**Fig. 4d**). Upon quantification of the co-localization of Vglut1 and Homer1, as expected, CTL neurons displayed higher co-localization of synaptic puncta (**Fig. 4e**, *Bonferroni* post-hoc test, *P<0.05). Furthermore, LiCl and LMK235-treated CDKL5 neurons displayed a significant increase in the number of co-localized puncta compared to CDKL5 untreated cells, indicating an increase in synaptogenesis (**Fig. 4e**, *Bonferroni* post-hoc test, *P<0.05). To determine if this partial recovery in synaptogenesis could rescue spontaneous neural activity, 4-week-old neurospheres were plated onto MEA plates, followed by chronic treatment for 3 weeks (**Fig. 4f**). Aligned raster plots of independent channels show that CTL neurons displayed higher spontaneous neural activity, as represented by number of spikes per min, compared to CDKL5 neurons (**Fig. 4g, 4h**, *Bonferroni* post-hoc test, *P<0.05). Although LiCl-treated CDKL5 neurons did not display any significant increase in spontaneous neural activity, LMK235-treated CDKL5 neurons showed a significantly higher number of spikes per min compared to untreated neurons (**Fig. 4g, 4h**, *Bonferroni* post-hoc test, *P<0.05). Together, our data suggests that decreases in synaptogenesis between CTL and CDKL5, that is manifested as a decrease in neural activity, can be rescued using LMK235.

DISCUSSION

Aberrant neuronal morphology is a feature present in neurons of patients with neurological disorders and has been studied in cellular models of disorders such as RTT (Armstrong et al., 1995; Kishi and Macklis, 2004). Investigating defects in neuronal morphology may provide insight into the disease pathology. Here, we examined dendritic outgrowth and complexity, such as arborization, from CDKL5 patient iPSC-derived neurons and found that CDKL5 neurons displayed significantly larger total dendritic lengths and arborization than CTL neurons *in vitro.* Our results show a trend contrasting previous rodent studies, which have shown loss of CDKL5 function to impair dendritic outgrowth, resulting in cortical neurons with a decreased total dendritic length compared to wild-type neurons (Amendola et al., 2014; Chen et al., 2010). A possible explanation for these opposite results is that CDKL5 function might not be completely conserved across species (Amendola et al., 2014). Evidence that could support the differential function of CDKL5 across rodents and humans is the inability of rodent models to recapitulate the seizure phenotype observed in humans in the absence of CDKL5 protein (Amendola et al., 2014; Wang et al., 2012). Moreover, the identification of 5 different CDKL5 isoforms in mouse and human, which displayed low homology (29-42%) at the 5' and 3' exonic ends and C-terminal domain, may also contribute to the observed differences (Hector et al., 2016).

The ability to generate hiPSC-derived neurons is significant because it provides a platform to study species-specific neurodevelopment in a dish and aberrations in neurodevelopment resulting from genetic mutations. Using human neurons have already provided a valuable tool to model neurological disorders because it retains the genetic

information from patients with specific mutations and circumvents issues associated with a lack of conserved gene function across species. However, the maturation potential and identity of iPSC-derived neurons differentiated *in vitro* remains a concern because transcriptional analysis has revealed that *in vitro* differentiated neurons consist primarily of cortical cells and reach maturity levels similar to that of a mid-fetus. This may be a concern in neurological disorders characterized by normal prenatal development, followed by postnatal onset because of whether iPSC-derived neurons retain neurological pathologies *in vitro* due to the maturity state that they are able to reach.

In order to circumvent any potential limitations placed by the maturity of *in vitro* differentiated neurons and to take advantage of an *in vivo* brain environment, we decided to integrate these two systems. The integration of human cells into the mouse brain has been reported and implicated as a model to study neurodevelopment in the context of a live brain environment (Espuny-Camacho et al., 2013; Muotri et al., 2005). Here, we engrafted human NPCs into neonatal mice to generate a chimeric human-mouse brain. We hoped to use the chimeric human-mouse brain as a platform to study neural development and aberrations resulting from neurological disorders while taking advantage of a live brain environment to potentially promote neuronal maturation beyond what is achievable from *in vitro* differentiation. After morphometric analysis, we found that defects in total dendritic length and arborization *in vitro* were retained *in vivo* in our chimeric human-mouse brain, validating our *in vitro* findings. These results suggest a cell autonomous influence of CDKL5 neurons in neuronal morphology as human CDKL5

neurons retained morphological defects despite being in the presence of a wild-type nervous system.

Utilizing hiPSC-derived neurons allowed us to test the safety and efficacy of a variety of compounds on a species-specific platform. Initially, the goal was to determine if nonsense mutations in the *CDKL5* locus could be overcome with read-through compounds that induce ribosomal read-through of nonsense mutations to recover the CDKL5 protein content. Although the mechanism of action of these compounds is unknown, they all act as nonsense codon suppressors, de-sensitizing ribosomes to termination codons by substituting a different amino acid in place of the nonsense codon, leading to the synthesis of a mature protein. Previous reports have shown that the use of antimicrobial aminoglycosides, such as gentamicin, has recovered the full-length CF transmembrane conductance regulator (CFTR) protein in models of Cystic Fibrosis (CF), as well as clinical trials (Howard et al., 1996; Wilschanski et al., 2003). Recovery of the CFTR protein restored activity in its cyclic AMP-activated chloride channel both *in vitro* and *in vivo* (Howard et al., 1996; Wilschanski et al., 2003). As promising as aminoglycosides are, its use is limited due to side effects resulting from chronic administration such as ototoxicity and nephrotoxicity. To overcome limitations in toxicity, non-aminoglycoside compounds were tested such as PTC124 (Ataluren/PTCA1046), a drug that is able to overcome nonsense codons in a manner similar to Gentamicin. Ataluren has recovered synthesis of full-length proteins as well as functional recovery (Tan et al., 2011). In addition to PTC124, other PTC compounds that

are not completely understood, but still promote ribosomal read-through of nonsense codons, were also used in this study.

After treatment, we detected very low levels of CDKL5 protein across all drugs. We deemed this to be insufficient and did not proceed to investigate whether these minimal increases could ameliorate any cellular or functional phenotypes. Furthermore, in an attempt to optimize drug concentrations, we tested the efficacy of the drugs after concentrating by 10-fold (data not shown). In this trial, we were still unable to detect any expression of CDKL5 and noticed cellular toxicity resulting from increasing the concentration. Rather than attempting to optimize and troubleshoot this approach, we switched our focus on whether we could rescue cellular or functional phenotypes associated with CDKL5 disorder such as decreases in synapse formation and neural activity.

Prior studies have shown that loss of CDKL5 mediated through RNAi or knock-out models have resulted in a decrease in synapse formation (Amendola et al., 2014; Chen et al., 2010). There were a variety of drugs selected on the basis that they have ameliorated disease phenotypes in other neurological disorders, known to pass the blood brain barrier, and are FDA approved. In order to determine if selected drugs could rescue synapse formation in CDKL5 neurons, we quantified the amount of co-localized pre-synaptic (Vglut1) and post-synaptic markers (Homer1) as an indicator of synapse formation. We found that treatment with LiCl and LMK235 partially rescued the number of synaptic puncta, as treated CDKL5 neurons displayed values significantly higher than untreated CDKL5 neurons.

Next, we wanted to determine if an increase in synaptogenesis could rescue spontaneous neural activity. Neurons exposed to LMK235 displayed a significant increase in the number of spikes, indicating that LMK235 rescued spontaneous neural activity that is compromised in CDKL5 neurons. Altogether, we report that LMK235 rescues defects in synaptogenesis and neural activity in CDKL5 neurons *in vitro*. Our findings align with previous literature as LMK235 was recently reported as a compound that rescues many neurological defects in a knock-out mouse model of CDKL5 such as synaptogenesis. CDKL5 mouse neurons displayed a decrease in synaptic connections that was restored with treatment of LMK235 (Trazzi et al., 2016), which is consistent with the synaptic rescue observed in our human neurons.

Using histone deacetylase inhibitors are valuable therapeutic targets for the treatment of many neurological disorders. However, HDAC inhibitors such as valproic acid have consequential side effects such as blocking neurogenesis and differentiation of NPCs. Additionally, other HDAC inhibitors induce global acetylation with many adverse side effects due to their non-specific nature. This indicates the need for therapeutic targets that are specific to disease pathology in order to diminish the side effects associated with unspecific inhibition.

LMK235 is a histone deacetylase inhibitor specific to HDAC4 and HDAC5, which is relevant because of its ability to treat pathologies specific to aberrations in HDAC4 and HDAC5 activity. Currently, there are no therapeutic targets or drugs to improve neurological phenotypes associated with CDKL5 disorder. We believe that the evidence from our study displaying a rescue in synaptogenesis and neural activity,

corroborated with the therapeutic benefits of LMK235 treatment in a CDKL5 knock-out mouse model, presents a potential therapeutic target for CDKL5 disorder.

The advent of hiPSCs provides a platform to study disease-relevant cell types that exhibit a patient's genetic background, including disease-relevant loci. This opportunity presents a major milestone and opportunity in the field of modeling neurodevelopmental disorders, as it allows for the generation of live human neurons from patients with specific mutations and the investigation of how this manifests as a functional, cellular or molecular phenotype. Engraftment of human cells into a live mouse brain environment provides an unprecedented opportunity to study human neurodevelopment *in vivo*. Furthermore, hiPSCs provide a platform to test, develop and tailor individual and effective therapies while overcoming interspecies differences. Ultimately, we hope our work will accelerate investigation of CDKL5 disease pathology and strengthen the pre-clinical testing platform, while reducing costs and increasing the success of clinical trials.

In this study, we successfully generated hiPSC-derived neurons from patients with CDKL5 disorder, allowing for the study and characterization of neurons containing patients' genetic information. With this, we uncovered and validated defects in neuronal morphology and synaptogenesis *in vitro*. Furthermore, taking advantage of a live mouse brain micro-environment, grafted human NPCs were allowed to develop and mature into neurons in the context of an *in vivo* brain to validate defects observed in neuronal morphology *in vitro*. Lastly, we validate a previously reported therapeutic compound for CDKL5 disorder in rodents that was able to rescue defects in synaptogenesis and neural electrical activity in human CDKL5 neurons.

FIGURES

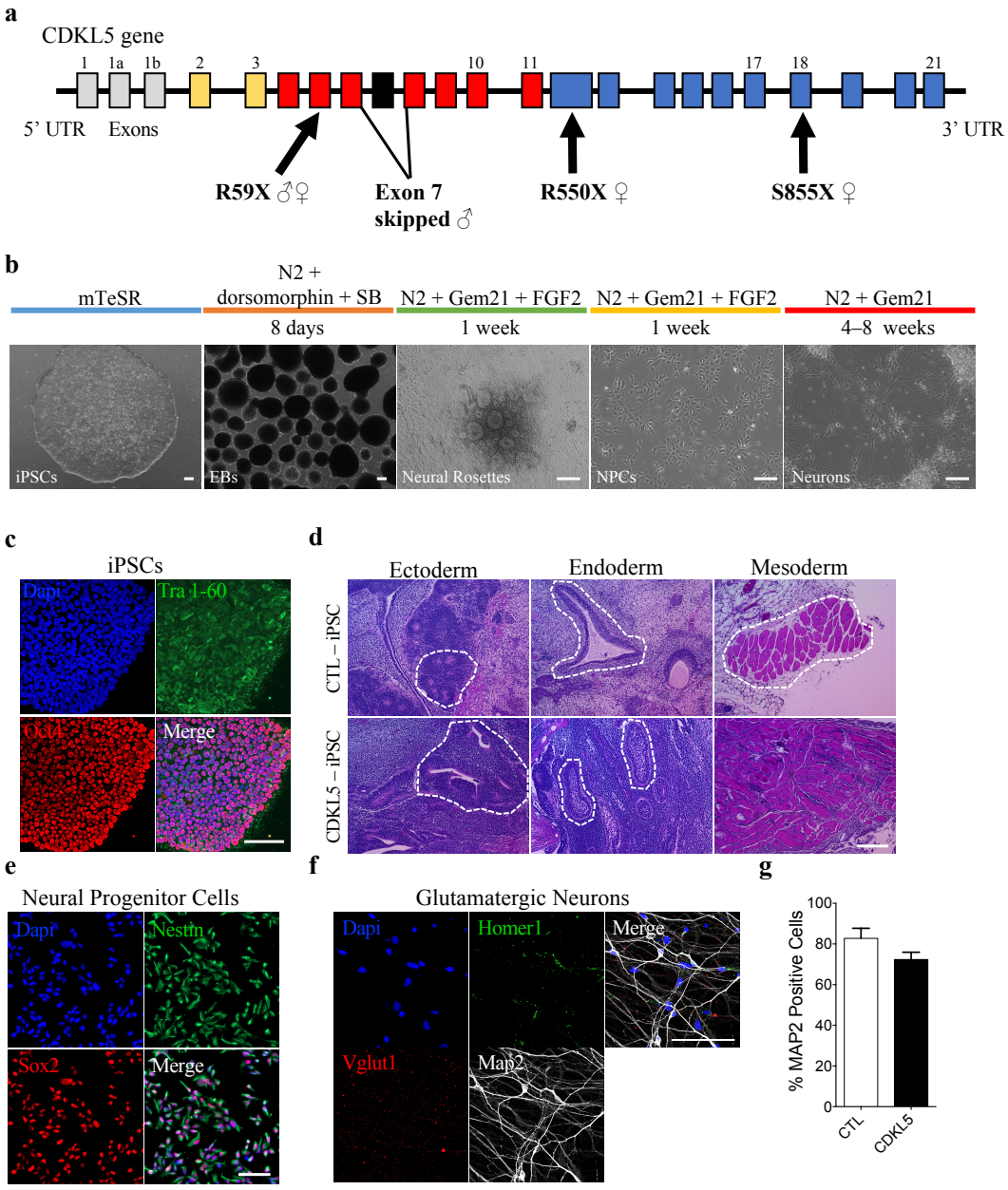

Figure 1. Characterization of differentiation potential of CDKL5 disorder patient-derived iPSCs. a, Schematic representation of the CDKL5 gene structure, amino acid mutations and gender in this study. Exons 1, 1a, 1b (gray) represent noncoding exons. Exons 2, 3 (yellow) represent the ATP binding site. Exons 4-6 and 8-11 (red) represent the serine/threonine kinase domain with Exon 7 (black) representing the kinase active site. Exons 12-21 (blue) represent the C-terminal domain. **b,** Neural induction and neuronal differentiation protocol. **c,** Representative immunofluorescent images displaying stage-specific protein expression in iPSCs. **d,** Representative images of H&E stains from iPSC-derived teratoma sections from CTL and CDKL5 patients. **e,** Representative immunofluorescent images displaying stage-specific protein expression in iPSC-derived NPCs. **f,** Representative immunofluorescent images displaying stage-specific protein expression in iPSC-derived glutamatergic neurons. **g,** Percentage of Map2-positive cells in neural cultures from CTL and CDKL5 patients. Map2 is a neuron-specific marker. n=3. n, number of cell lines. All scale bars represent 100 µm.

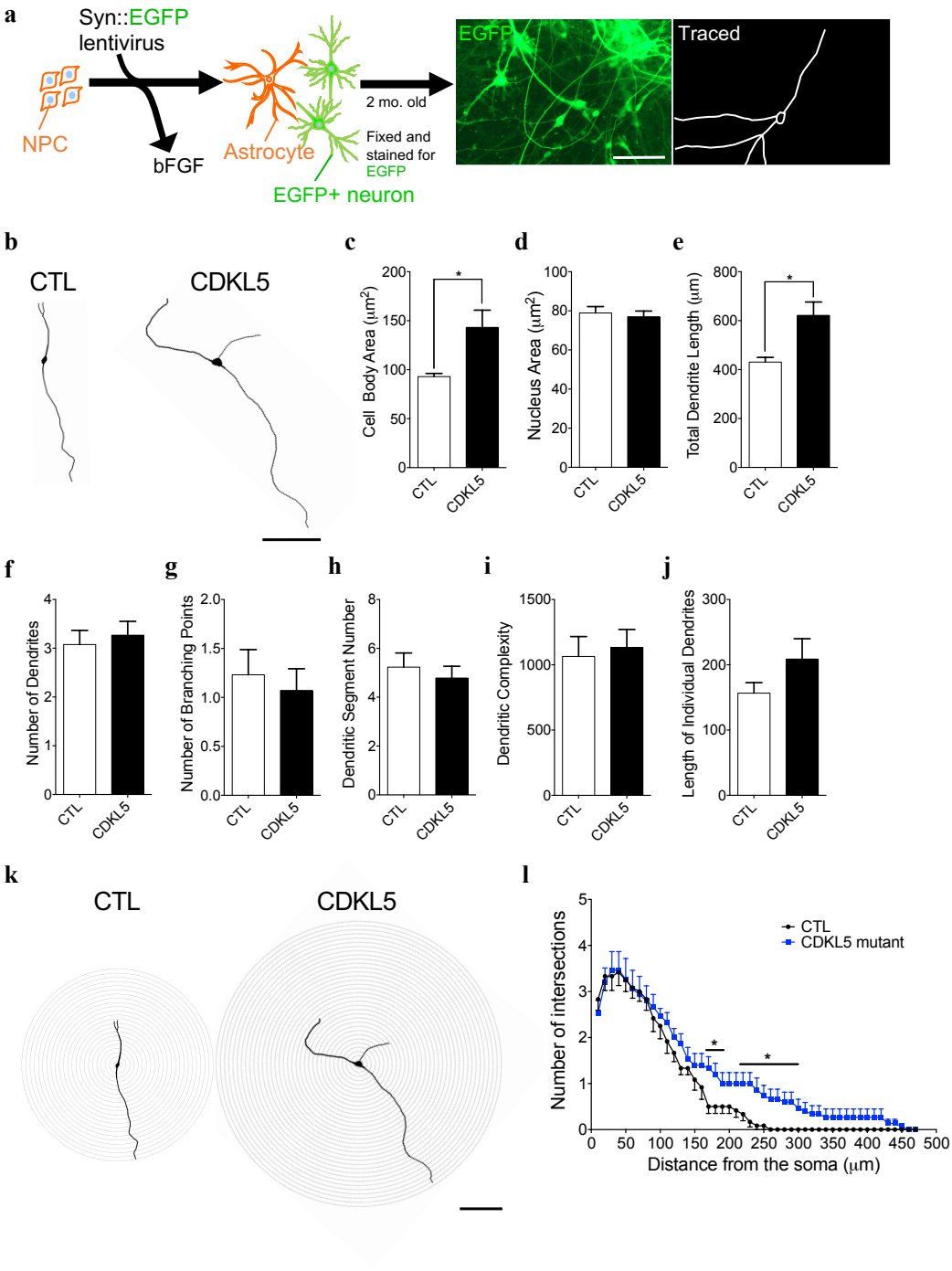

Figure 2. Altered morphology of CDKL5 disorder iPSC-derived neurons *in vitro.* **a**, Summary of preparation of neurons for evaluation by morphometric analysis. **b,** Representative images of neuron tracings from CTL and CDKL5 disorder patients that were differentiated for 8 weeks (Syn::EGFP neurons). **c-j,** Morphometric analyses showing a significant difference between CTL and CDKL5 in cell body area (**c**), total dendrite length (**e**). **k,** Sholl analysis diagrams of representative images of neuron tracings. Concentric circles have a distance of 10 μm between them. **l**, Sholl analysis of CTL and CDKL5 disorder neurons. Data are shown as mean ± s.e.m.; n=14. n, number of traced neurons per condition. *P<0.05, two-tailed unpaired t-test. All scale bars represent 100 μm.

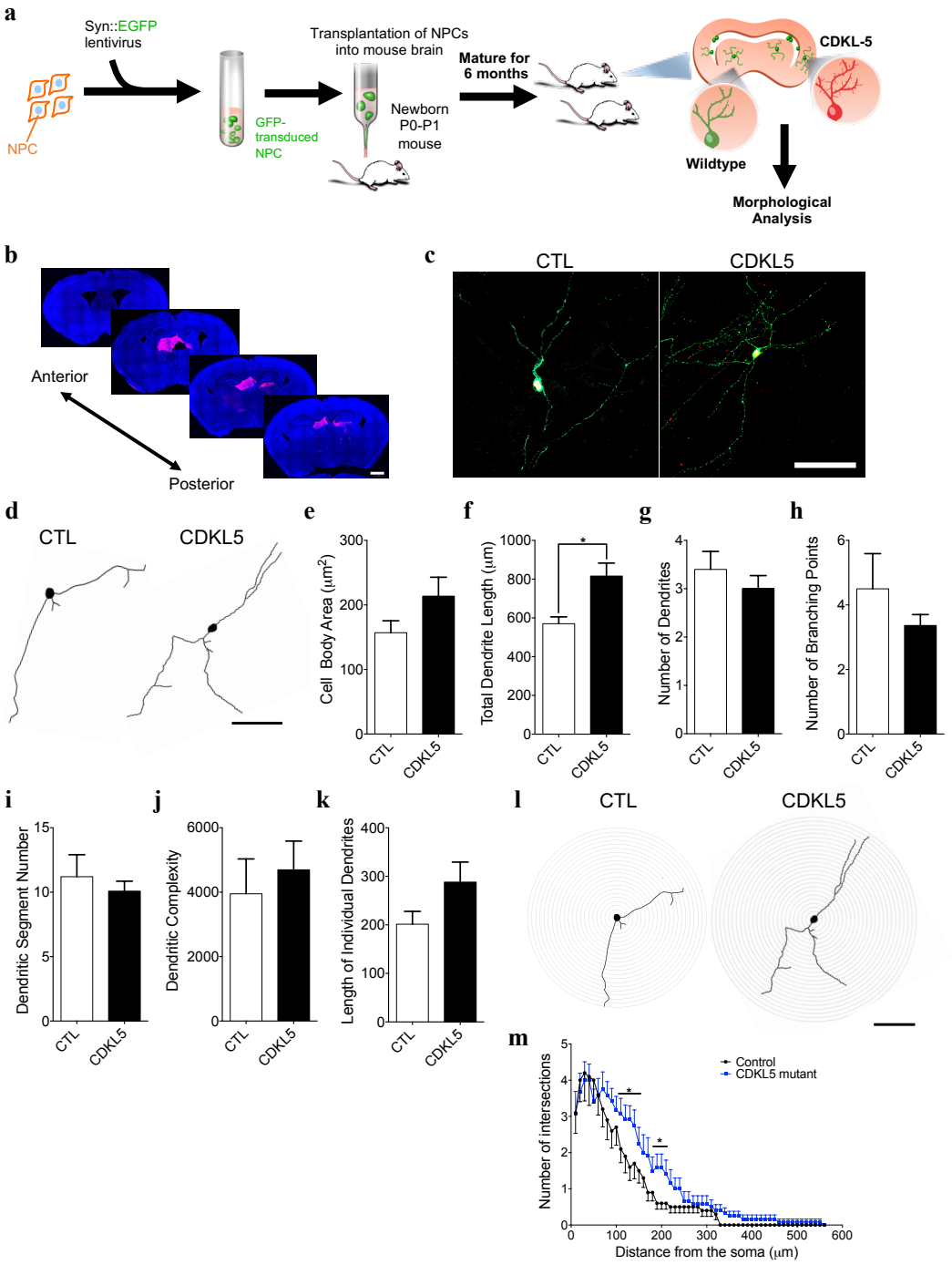

Figure 3. Altered morphology of CDKL5 disorder iPSC-derived neurons *in vivo*. a, Summary of preparation and transplantation protocol of Syn::EGFP NPCs into immunodeficient mice for evaluation by morphometric analysis. **b,** Mouse brain sections with HuNu-positive cells (red) from anterior to posterior. Scale bar represents 1000 μm. **c,** Representative immunofluorescent images of human neurons from chimeric mouse brain after 6-month differentiation. **d,** Representative images of neuron tracings from CTL and CDKL5 disorder patients that were differentiated for 6 months inside of immunodeficient NOD/SCID mice (Syn::EGFP neurons). **e-k,** Morphometric analyses showing a significant difference between CTL and CDKL5 in total dendrite length (**f**). **l,** Sholl analysis diagrams of representative images of neuron tracings. Concentric circles have a distance of 10 μm between them. **m,** Sholl analysis of CTL and CDKL5 disorder neurons. Data are shown as mean ± s.e.m.; n=12. n, number of traced neurons per condition. *P<0.05, two-tailed unpaired t-test. All scale bars represent 100 μm (except **b**).

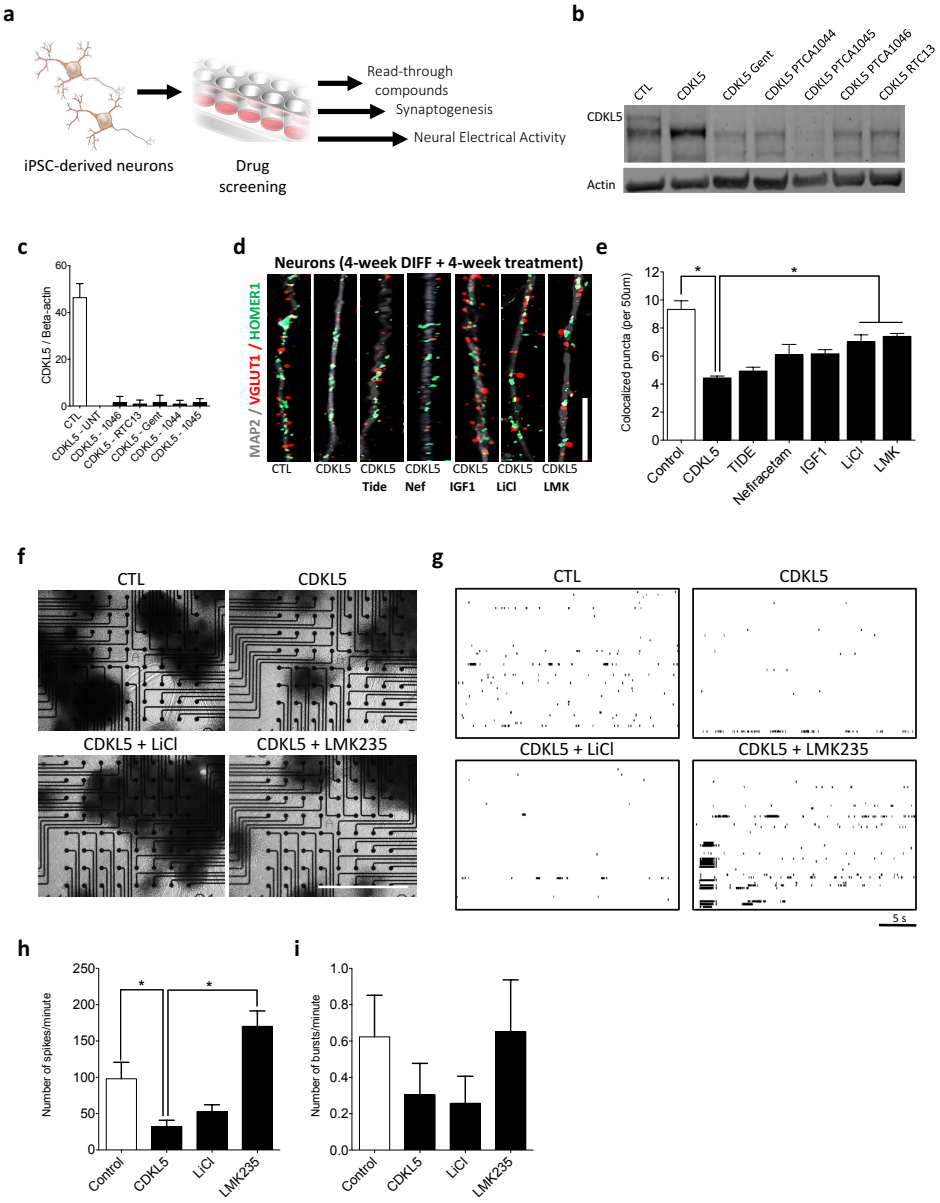

Figure 4. *In vitro* drug treatment of hiPSC-derived neurons. a, Summary of experimental goals/readouts. **b,** Western Blot results after differentiation of iPSC-derived neurons for 4 weeks, adding read-through compounds and collecting cells 48 hours later. Extracted protein was blotted for CDKL5 and Actin. **c,** Quantification of Western Blot displaying relative CDKL5 protein amount from varying treatments and conditions. Amount of CDKL5 is normalized to Actin. **d,** Representative immunofluorescent images of dendrites stained for Map2, Vglut1 (pre-synaptic marker), and Homer1 (post-synaptic marker) from neuronal cultures that were differentiated for 4 weeks, followed by 4 weeks of chronic drug treatment. Scale bar represents 10 µm. **e,** Quantification of co-localization of synaptic puncta, Vglut1 and Homer1. Data are shown as mean ± s.e.m; n=3. n, number of cell lines and their related controls used. One-way ANOVA and Bonferroni's multiple comparisons test. *P<0.05. **f,** Representative images of neurons on MEA plates. Scale bars represent 1000 µm. **g,** Raster plots from varying conditions. Spontaneous activity is shown for a period of 30 s. Scale bar represents 5 s. **h,** Number of spikes per min from varying conditions. Data are shown as mean ± s.e.m; n=3. n, number of cell lines and their related controls used. One-way ANOVA and Bonferroni's multiple comparisons test. *P<0.05. **i,** Number of bursts over a 3 min recording from varying conditions. 10 spikes in 100 ms constituted a network burst. Data are shown as mean ± s.e.m; n=3. n, number of cell lines and their related controls used.

TABLES

Table 1. CDKL5 patient cohort information and related controls.

Patient iPSC Name	Sex	Diagnosis	Mutation	Age (years)	Relationship	Affected Exon
3	Female	CDKL5	R59X	3	Daughter	5
4	Female	Control	None	41	Mother of patient 3	None
10	Male	CDKL5	R59X	15	Son	5
11	Male	Control	None	35	Father of patient 10	None
91	Male	CDKL5	c.404-1G>A (splice mutation; p.D135_F154del, exon 7 skipping)	4	Son	7
101	Male	Control	None	38	Father of patient 91	None
122C1	Female	CDKL5	R550X	3	Patient 122	12
122C2	Female	CDKL5	None	3	Isogenic control of patient 122	None
130C1	Female	CDKL5	c.2564C>G (p.S855X) nonsense (serine>UGA)	7	Patient 130	18
130C2	Female	CDKL5	None	7	Isogenic control of patient 130	None

Table 2. Final concentration and description of drugs

Drug	Final concentration	Description
Gentamicin	200 µg//ml	• Read-through drugs
PTCA1044	5 nM	
PTCA1045	8 µM	
PTCA1046	80 µM	
RTC13	100 µM	
IGF-1	50 µg/ml	• Activator of AKT signaling pathway, a stimulator of cell growth and proliferation, and a potent inhibitor of apoptosis • Shown to improve symptoms in MeCP2 mouse and human models such as synaptogenesis
LiCl	1 mM	• A salt used in psychiatric medication for bipolar disorder, major depression and schizophrenia
LMK235	2 nM	• Inhibitor of HDAC4 • Shown to symptoms such as neurite outgrowth and synaptogenesis in CDKL5 KO mouse model
Tideglusib	1 µM	• Inhibitor of GSK-3 pathway • Other GSK3β inhibitors shown to improve development and learning in CDKL5 mouse models
Nefiracetam	1 µM	• Activates L/N-type calcium channels, cholinergic, monoaminergic, and GABAergic systems. • Cognitive enhancer shown to be neuroprotetive in animal models

REFERENCES

Amendola, E., Zhan, Y., Mattucci, C., Castroflorio, E., Calcagno, E., Fuchs, C., Lonetti, G., Silingardi, D., Vyssotski, A.L., Farley, D., Ciani, E., Pizzorusso, T., Giustetto, M., Gross, C.T., 2014. Mapping pathological phenotypes in a mouse model of CDKL5 disorder. PLoS One 9, 5–16. doi:10.1371/journal.pone.0091613

Armstrong, D., Dunn, J.K., Antalffy, B., Trivedi, R., 1995. Selective Dendritic Alterations in the Cortex of Rett Syndrome. J. Neuropathol. Exp. Neurol. 54, 195–201. doi:10.1097/00005072-199503000-00006

Chailangkarn, T., Trujillo, C.A., Freitas, B.C., Hrvoj-Mihic, B., Herai, R.H., Yu, D.X., Brown, T.T., Marchetto, M.C., Bardy, C., McHenry, L., Stefanacci, L., Järvinen, A., Searcy, Y.M., DeWitt, M., Wong, W., Lai, P., Ard, M.C., Hanson, K.L., Romero, S., Jacobs, B., Dale, A.M., Dai, L., Korenberg, J.R., Gage, F.H., Bellugi, U., Halgren, E., Semendeferi, K., Muotri, A.R., 2016. A human neurodevelopmental model for Williams syndrome. Nature In press, 1–25. doi:10.1038/nature19067

Chambers, S.M., Fasano, C.A., Papapetrou, E.P., Tomishima, M., Sadelain, M., Studer, L., 2009. Highly efficient neural conversion of human ES and iPS cells by dual inhibition of SMAD signaling. Nat. Biotechnol. 27, 275–280. doi:10.1038/nbt.1529

Chen, Q., Zhu, Y.-C., Yu, J., Miao, S., Zheng, J., Xu, L., Zhou, Y., Li, D., Zhang, C., Tao, J., Xiong, Z.-Q., 2010. CDKL5, a Protein Associated with Rett Syndrome, Regulates Neuronal Morphogenesis via Rac1 Signaling. J. Neurosci. 30, 12777–12786. doi:10.1523/JNEUROSCI.1102-10.2010

Dragunow, M., 2008. The adult human brain in preclinical drug development. Nat. Rev. Drug Discov. 7, 659–666. doi:10.1038/nrd2617

Espuny-Camacho, I., Michelsen, K.A., Gall, D., Linaro, D., Hasche, A., Bonnefont, J., Bali, C., Orduz, D., Bilheu, A., Herpoel, A., Lambert, N., Gaspard, N., Péron, S., Schiffmann, S.N., Giugliano, M., Gaillard, A., Vanderhaeghen, P., 2013. Pyramidal Neurons Derived from Human Pluripotent Stem Cells Integrate Efficiently into Mouse Brain Circuits In Vivo. Neuron 77, 440–456. doi:10.1016/j.neuron.2012.12.011

Fehr, S., Wilson, M., Downs, J., Williams, S., Murgia, A., Sartori, S., Vecchi, M., Ho, G., Polli, R., Psoni, S., Bao, X., de Klerk, N., Leonard, H., Christodoulou, J., 2012. The CDKL5 disorder is an independent clinical entity associated with early-onset encephalopathy. Eur. J. Hum. Genet. 21, 266–73. doi:10.1038/ejhg.2012.156

Fichou, Y., Nectoux, J., Bahi-Buisson, N., Chelly, J., Bienvenu, T., 2011. An isoform of the severe encephalopathy-related CDKL5 gene, including a novel exon with extremely high sequence conservation, is specifically expressed in brain. J. Hum.

Genet. 56, 52–57. doi:10.1038/jhg.2010.143

Hector, R.D., Dando, O., Landsberger, N., Kilstrup-Nielsen, C., Kind, P.C., Bailey, M.E.S., Cobb, S.R., 2016. Characterisation of CDKL5 Transcript Isoforms in Human and Mouse. PLoS One 11, e0157758. doi:10.1371/journal.pone.0157758

Henderson, C., Wijetunge, L., Kinoshita, M.N., Shumway, M., Hammond, R.S., Postma, F.R., Brynczka, C., Rush, R., Thomas, a., Paylor, R., Warren, S.T., Vanderklish, P.W., Kind, P.C., Carpenter, R.L., Bear, M.F., Healy, a. M., 2012. Reversal of Disease-Related Pathologies in the Fragile X Mouse Model by Selective Activation of GABAB Receptors with Arbaclofen. Sci. Transl. Med. 4, 152ra128-152ra128. doi:10.1126/scitranslmed.3004218

Howard, M., Frizzell, R.A., Bedwell, D.M., 1996. Aminoglycoside antibiotics restore CFTR function by overcoming premature stop mutations. Nat. Med. 2, 467–9. doi:10.1038/nm0496-467

Johnston, S.F. and M., 2005. Whither Model Organism Research? Science (80-.). 307, 1885–1886. doi:10.1126/science.1108872

Kalscheuer, V.M., Tao, J., Donnelly, A., Hollway, G., Schwinger, E., Kübart, S., Menzel, C., Hoeltzenbein, M., Tommerup, N., Eyre, H., Harbord, M., Haan, E., Sutherland, G.R., Ropers, H.-H., Gécz, J., K?bart, S., Menzel, C., Hoeltzenbein, M., Tommerup, N., Eyre, H., Harbord, M., Haan, E., Sutherland, G.R., Ropers, H.-H., G?cz, J., 2003. Disruption of the Serine/Threonine Kinase 9 Gene Causes Severe X-Linked Infantile Spasms and Mental Retardation. Am. J. Hum. Genet. 72, 1401–1411. doi:10.1086/375538

Kameshita, I., Sekiguchi, M., Hamasaki, D., Sugiyama, Y., Hatano, N., Suetake, I., Tajima, S., Sueyoshi, N., 2008. Cyclin-dependent kinase-like 5 binds and phosphorylates DNA methyltransferase 1. Biochem. Biophys. Res. Commun. 377, 1162–1167. doi:10.1016/j.bbrc.2008.10.113

Kishi, N., Macklis, J.D., 2004. MECP2 is progressively expressed in post-migratory neurons and is involved in neuronal maturation rather than cell fate decisions. Mol. Cell. Neurosci. 27, 306–321. doi:10.1016/j.mcn.2004.07.006

Liang, N., Trujillo, C.A., Negraes, P.D., Muotri, A.R., Lameu, C., Ulrich, H., 2017. Stem cell contributions to neurological disease modeling and personalized medicine. Prog. Neuro-Psychopharmacology Biol. Psychiatry 1–9. doi:10.1016/j.pnpbp.2017.05.025

Lin, C., Franco, B., Rosner, M.R., 2005. CDKL5/Stk9 kinase inactivation is associated with neuronal developmental disorders. Hum. Mol. Genet. 14, 3775–3786. doi:10.1093/hmg/ddi391

Marchetto, M.C.N., Carromeu, C., Acab, A., Yu, D., Yeo, G.W., Mu, Y., Chen, G., Gage, F.H., Muotri, A.R., 2010. A Model for Neural Development and Treatment of Rett Syndrome Using Human Induced Pluripotent Stem Cells. Cell 143, 527–539. doi:10.1016/j.cell.2010.10.016

Mari, F., Azimonti, S., Bertani, I., Bolognese, F., Colombo, E., Caselli, R., Scala, E., Longo, I., Grosso, S., Pescucci, C., Ariani, F., Hayek, G., Balestri, P., Bergo, A., Badaracco, G., Zappella, M., Broccoli, V., Renieri, A., Kilstrup-Nielsen, C., Landsberger, N., 2005. CDKL5 belongs to the same molecular pathway of MeCP2 and it is responsible for the early-onset seizure variant of Rett syndrome. Hum. Mol. Genet. 14, 1935–1946. doi:10.1093/hmg/ddi198

McAllister, A.K., Lo, D.C., Katz, L.C., 1995. Neurotrophins regulate dendritic growth in developing visual cortex. Neuron 15, 791–803.

Muotri, A.R., Nakashima, K., Toni, N., Sandler, V.M., Gage, F.H., 2005. Development of functional human embryonic stem cell-derived neurons in mouse brain. Proc. Natl. Acad. Sci. 102, 18644–18648. doi:10.1073/pnas.0509315102

Nageshappa, S., Carromeu, C., Trujillo, C.A., Mesci, P., Pasciuto, E., Vanderhaeghen, P., Espuny-Camacho, I., Verfaillie, C.M., Raitano, S., Kumar, A., Carvalho, C.M.B., Bagni, C., Ramocki, M.B., Araujo, B.H.S., Torres, L.B., Lupski, J.R., Van Esch, H., Muotri, A.R., 2015. Altered neuronal network and rescue in a human MECP2 duplication model. Mol Psychiatry 21, 1–11. doi:10.1038/mp.2015.128

Ricciardi, S., Ungaro, F., Hambrock, M., Rademacher, N., Stefanelli, G., Brambilla, D., Sessa, A., Magagnotti, C., Bachi, A., Giarda, E., Verpelli, C., Kilstrup-Nielsen, C., Sala, C., Kalscheuer, V.M., Broccoli, V., 2012. CDKL5 ensures excitatory synapse stability by reinforcing NGL-1-PSD95 interaction in the postsynaptic compartment and is impaired in patient iPSC-derived neurons. Nat. Cell Biol. 14, 911–23. doi:10.1038/ncb2566

Rusconi, L., Salvatoni, L., Giudici, L., Bertani, I., Kilstrup-Nielsen, C., Broccoli, V., Landsberger, N., 2008. CDKL5 expression is modulated during neuronal development and its subcellular distribution is tightly regulated by the C-terminal tail. J. Biol. Chem. 283, 30101–30111. doi:10.1074/jbc.M804613200

Stein, J.L., de la Torre-Ubieta, L., Tian, Y., Parikshak, N.N., Hernández, I.A., Marchetto, M.C., Baker, D.K., Lu, D., Hinman, C.R., Lowe, J.K., Wexler, E.M., Muotri, A.R., Gage, F.H., Kosik, K.S., Geschwind, D.H., 2014. A quantitative framework to evaluate modeling of cortical development by neural stem cells. Neuron 83, 69–86. doi:10.1016/j.neuron.2014.05.035

Takahashi, K., Tanabe, K., Ohnuki, M., Narita, M., Ichisaka, T., Tomoda, K., Yamanaka, S., 2007. Induction of Pluripotent Stem Cells from Adult Human Fibroblasts by

Defined Factors. Cell 131, 861–872. doi:10.1016/j.cell.2007.11.019

Tan, L., Narayan, S.B., Chen, J., Meyers, G.D., Bennett, M.J., 2011. PTC124 improves readthrough and increases enzymatic activity of the CPT1A R160X nonsense mutation. J. Inherit. Metab. Dis. 34, 443–447. doi:10.1007/s10545-010-9265-5

Thomson, J.A., Itskovitz-Eldor, J., Shapiro, S.S., Waknitz, M.A., Swiergiel, J.J., Marshall, V.S., Jones, J.M., 1998. Embryonic stem cell lines derived from human blastocysts. Science 282, 1145–7. doi:10.1126/science.282.5391.1145

Trazzi, S., Fuchs, C., Viggiano, R., De Franceschi, M., Valli, E., Jedynak, P., Hansen, F.K., Perini, G., Rimondini, R., Kurz, T., Bartesaghi, R., Ciani, E., 2016. HDAC4: a key factor underlying brain developmental alterations in CDKL5 disorder. Hum. Mol. Genet. 25, 3887–3907. doi:10.1093/hmg/ddw231

Tropea, D., Giacometti, E., Wilson, N.R., Beard, C., McCurry, C., Fu, D.D., Flannery, R., Jaenisch, R., Sur, M., 2009. Partial reversal of Rett Syndrome-like symptoms in MeCP2 mutant mice. Proc. Natl. Acad. Sci. 106, 2029–2034. doi:10.1073/pnas.0812394106

Wang, I.-T.J., Allen, M., Goffin, D., Zhu, X., Fairless, A.H., Brodkin, E.S., Siegel, S.J., Marsh, E.D., Blendy, J. a, Zhou, Z., 2012. Loss of CDKL5 disrupts kinome profile and event-related potentials leading to autistic-like phenotypes in mice. Proc. Natl. Acad. Sci. U. S. A. 109, 21516–21. doi:10.1073/pnas.1216988110

Watase, K., Zoghbi, H.Y., 2003. Modelling brain diseases in mice: the challenges of design and analysis. Nat. Rev. Genet. 4, 296–307. doi:10.1038/nrg1045

Williamson, S.L., Giudici, L., Kilstrup-Nielsen, C., Gold, W., Pelka, G.J., Tam, P.P.L., Grimm, A., Prodi, D., Landsberger, N., Christodoulou, J., 2012. A novel transcript of cyclin-dependent kinase-like 5 (CDKL5) has an alternative C-terminus and is the predominant transcript in brain. Hum. Genet. 131, 187–200. doi:10.1007/s00439-011-1058-x

Wilschanski, M., Yahav, Y., Yaacov, Y., Blau, H., Bentur, L., Rivlin, J., Aviram, M., Bdolah-Abram, T., Bebok, Z., Shushi, L., Kerem, B., Kerem, E., 2003. Gentamicin-induced correction of CFTR function in patients with cystic fibrosis and CFTR stop mutations. N. Engl. J. Med. 349, 1433–1441. doi:10.1056/NEJMoa022170

Zhu, Y.-C., Li, D., Wang, L., Lu, B., Zheng, J., Zhao, S.-L., Zeng, R., Xiong, Z.-Q., 2013. Palmitoylation-dependent CDKL5-PSD-95 interaction regulates synaptic targeting of CDKL5 and dendritic spine development. Proc. Natl. Acad. Sci. U. S. A. 110, 9118–23. doi:10.1073/pnas.1300003110